JACS
JOURNAL OF THE AMERICAN CHEMICAL SOCIETY

Communication

pubs.acs.org/JACS

Aspartame-Stabilized Gold–Silver Bimetallic Biocompatible Nanostructures with Plasmonic Photothermal Properties, Antibacterial Activity, and Long-Term Stability

Chiara Fasciani,[†] M. Jazmin Silvero,[†,‡] Maria Alexandra Anghel,[†] Gerardo A. Argüello,[‡] Maria Cecilia Becerra,[§] and Juan C. Scaiano*[,†]

[†]Department of Chemistry and Centre for Catalysis Research and Innovation, University of Ottawa, Ottawa, Ontario K1N 6N5, Canada

[‡]Facultad de Ciencias Químicas, Universidad Nacional de Córdoba, 5000 Córdoba, Argentina

[§]Instituto Multidisciplinario de Biología Vegetal (CONICET), Departamento de Farmacia, Universidad Nacional de Córdoba, 5000 Córdoba, Argentina

Supporting Information

ABSTRACT: Gold–silver core–shell nanoparticles stabilized with a common sweetener, aspartame (AuNP@Ag@Asm), combine the antimicrobial properties of silver with the photoinduced plasmon-mediated photothermal effects of gold. The particles were tested with several bacterial strains, while biocompatibility was verified with human dermal fibroblasts.

When a metal nanoparticle interacts with light of a wavelength longer than the dimensions of the particle itself, a Surface Plasmon Resonance (SPR) phenomenon can lead to characteristic light absorption due to the coherent oscillation of the surface electrons induced by the light.[1] Particularly interesting are the cases of gold, silver and copper, where the SPR absorptions occur in the visible range. Variation on the region of absorption can be achieved by changing the size, shape, or composition of the particles.[2] This effect has been investigated and used for several applications, which range from catalysis[3] to biochemistry.[4,5]

Three known properties of noble metal nanoparticles stimulated the research reported here: (a) Upon light absorption gold nanoparticles (AuNP) can deliver energy with pinpoint precision,[6] with high efficiency, and in subpicosecond time scales. This property has been proposed as a powerful tool for photodynamic therapy (PDT), a light-mediated form of clinical treatment.[4,7] (b) Silver nanoparticles (AgNP) have excellent antimicrobial properties that exceed those of silver ions themselves, and it has been proposed that the AgNP themselves are strongly anti-infective, beyond any effect due to Ag^+ leaching.[8,9] And (c) peptides, such as LL37, can stabilize metal nanoparticles, such as AgNP, while they retain their anti-infective properties and show excellent biocompatibility.[10] Based on this observation, we present here the remarkable behavior of core–shell gold–silver nanostructures stabilized with aspartame (Asm), a common artificial sweetener (Figure 1).

The material presented in this contribution consists of a gold core, encapsulated in a silver shell[11,12] and stabilized with a dipeptide, specifically aspartame. The gold core has been chosen for the purpose of efficient heat delivery through established plasmonic mechanisms.[13] The silver shell retains the antibacterial properties that have been characterized for AgNP. The surface protection with aspartame leads to excellent aqueous stabilization with a long shelf life. Further, aspartame is nontoxic,[14] remarkably inexpensive, and easy to replace if other molecules with specific biological targets are desirable for surface coating. Moreover, in addition to the synthesis and characterization of aspartame stabilized Au/Ag nanostructures (AuNP@Ag@Asm), representative *in vitro* experiments were carried out as a first indication of their antibacterial properties. Indeed, the effect of light activation and their biocompatibility were tested with primary human dermal fibroblasts (ATCC).

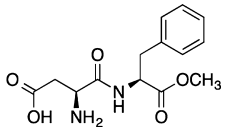

Figure 1. Aspartame molecular structure.

AuNP seeds (~12 nm) were used for seed-mediated growth of core–shell nanoparticles.[15] The synthesis of AuNP seeds was done via an established procedure.[11] Briefly, an aqueous solution of 0.33 mM $HAuCl_4$ and 1 mM I-2959 (1:3 stoichiometric ratio) was irradiated with UVA light, using a Luzchem LZC-4 photoirradiator, for 15 min (Scheme 1). After irradiation, the solution was left in the dark for at least 24 h before surface functionalization with silver. A seed-mediated growth procedure was employed for the formation of Au/Ag core–shell nanoparticles according to a reported procedure,[11] but by replacing the citrate stabilizer with two biocompatible stabilizing agents, aspartame, as indicated above, and LL37. We emphasize here the results with aspartame. The concentration of $AgNO_3$ was chosen to have nanoparticles in which the core represents the same metal loading with respect to the shell (Au/Ag = 50/50). Briefly, an aqueous solution of 110 μM $AgNO_3$, 4 μM of aspartame, and 110 μM I-2959 was purged under N_2 for 45 min. After purging, 1 mL of AuNP seeds was added to the cuvette and irradiated for 15

Received: October 10, 2014
Published: December 3, 2014

 © 2014 American Chemical Society dx.doi.org/10.1021/ja510435u | J. Am. Chem. Soc. 2014, 136, 17394–17397

Scheme 1. I-2959 Photolysis and Metal Ion Reduction That Subsequently Leads to Metal Nanoparticle Formation

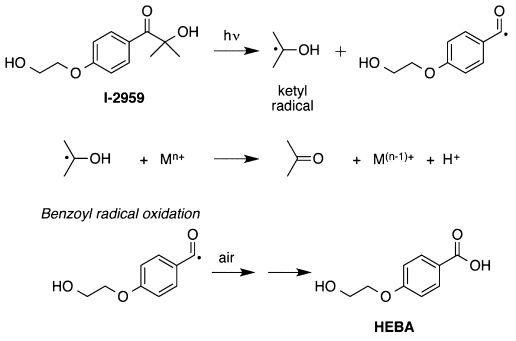

min with UVA light. Absorbance spectra were taken before and after irradiation, as reported below.

Formation of AuNP@Ag@Asm led to the spectral changes in Figure 2. Note that after irradiation with $AgNO_3$ the band

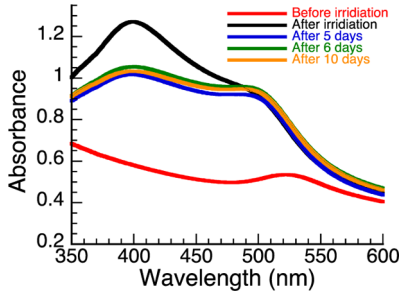

Figure 2. Absorption spectra for core−shell nanoparticles stabilized with aspartame (AuNP@Ag@Asm), recorded before irradiation (red trace), right after irradiation in the presence of $AgNO_3$ (black trace), and at different times after the irradiation was completed (blue to orange traces). The maxima of the two bands obtained after irradiation are centered at 405 and 510 nm.

corresponding to the Au plasmon absorption is shifted to the blue, while a new band, corresponding to the Ag plasmon absorption and centered at 405 nm, appears. The intensity of the two absorptions is consistent with the presence of comparable amounts of Au and Ag. Moreover, after the initial stabilization of the particles formed, the UV spectra did not change with time, showing very high stability. The analysis of the UV−vis spectra furnished a clear indication that core−shell structures are formed as opposed to separate nanoparticles or alloys. Indeed, in those cases we would have had no shift of the plasmon maximum (single particles) or a single band between the two metal plasmon absorptions (alloy).[16]

In order to establish the structure and size of AuNP@Ag@Asm particles, TEM images were taken and analyzed for different samples. The images obtained clearly reveal that AuNP@Ag@Asm particles are spherical with an average diameter of 16.6 ± 4.7 nm (n = 497). The particles present a darker central region, attributed to the gold core, as well a lighter section around it, representing the silver shell; see Figure 3.

EDS analysis was performed for AuNP@Ag@Asm, and the relative average percent (%) composition revealed 45.8 ± 1.6% silver and 54.2 ± 1.7% gold, similar to the anticipated composition based on the amount of $HAuCl_4$ (110 μM) and silver nitrate (110 μM) respectively. The EDS spectra, reported in the Supporting Information (SI), confirmed the metal composition of the core−shell particles formed. The presence

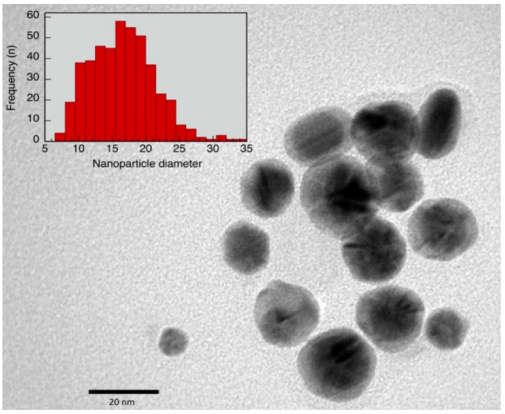

Figure 3. Transmission electron microscope image for AuNP@Ag@Asm. The scale bar of the image represents 20 nm. Core−shell nature of the nanoparticles can be easily visualized. The inset represents a histogram of the size distribution of the nanoparticles, which yields a mean diameter of ∼17 nm (n = 497).

of traces of carbon and chlorine ions was also detected, attributable to residues of the byproduct 4-hydroxyethoxybenzoic acid (HEBA) and the starting material $HAuCl_4$, respectively. The presence of HEBA in these materials is well established.[11,17]

In addition, the antimicrobial properties of the particles synthesized were tested, by performing Minimal Inhibitory Concentration (MIC) experiments via a microdilution assay. Information regarding the setup used is reported in the SI. Briefly, two identical 96-well plates were prepared using particle concentrations in the range of 0−25 μM. The choice of the concentrations was based on the hypothesis that AuNP@Ag@Asm would have somewhat similar MIC values to other silver-containing particles.[10] Three different bacteria strains, *Staphylococcus aureus* ATTC 25923, *Staphylococcus epidermidis* SE19, and *Escherichia coli* CF073, were analyzed. Parallel experiments of identical plates in the dark or under 530 nm LED irradiation were held for 18 h at 37°C, and the resulting OD of the bacterial suspensions was measured.

The results obtained for each strain analyzed are reported in Figure 4.

In the presence of AuNP@Ag@Asm the MIC value is lower for irradiated experiments than nonirradiated experiments. Therefore, the amount of AuNP@Ag@Asm needed to inhibit bacterial growth is lower under light exposure. This effect can be due to either the irradiation itself or the heat emitted by the AuNP@Ag@Asm from plasmon excitation at 530 nm. To verify that it is in fact the photothermal properties of the gold core causing microbial inhibition, control experiments were performed. In each experiment, the measurement of the OD in the absence of nanoparticles was taken, and significant bacterial density was visualized in both irradiated and nonirradiated conditions. Therefore, the lower MIC value for irradiated experiments should be attributed to the synergistic effect of the photothermal properties of gold and the antimicrobial action of the silver shell and not to the direct cell irradiation effect. Note that 530 nm irradiation of AgNP (no gold) does not enhance their antibacterial properties (see p S9 in the SI).

A summary of the results obtained is presented in Table 1 for further comparison. It was reported that AuNP by themselves need a higher concentration to completely inhibit microbial growth.[18] In order to decrease the MIC of gold nanoparticles, a shell of material with well-known antibacterial properties was

dx.doi.org/10.1021/ja510435u | J. Am. Chem. Soc. 2014, 136, 17394−17397

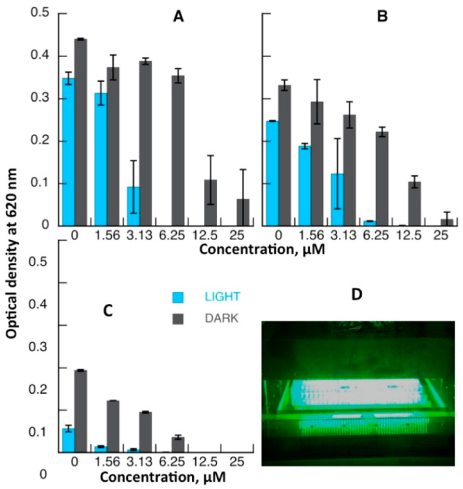

Figure 4. Concentration dependent graphs depicting microbial inhibition action by AuNP@Ag@Asm via measurement of the optical density for *E. coli* (A), *S. aureus* (B), and *S. epidermidis* (C). The legend denotes experiments as either irradiated (LIGHT) or nonirradiated (DARK). Optical density measurements were taken at 620 nm. Panel D shows the experimental setup, with the well plate under intense LED illumination.

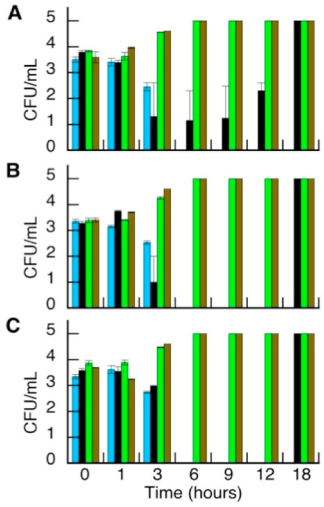

Figure 5. Time−kill curves recorded at $t = 0, 1, 3, 6, 9$, and 18 h, for *E. coli* (A), *S. aureus* (B), and *S. epidermidis* (C). The experiments were conducted using AuNP@Ag@Asm at MIC concentration, under 530 nm irradiation (blue traces) and in the dark (black traces). Controls experiments in absence of AuNP@Ag@Asm were also performed under irradiation (green trace) and in the dark (brown traces).

Table 1. Cumulative Minimal Inhibitory Concentration Results (μM) from the Analysis of MIC Data[a]

	AuNP[b]		AuNP@Ag@LL37		AuNP@Ag@Asm	
bacterial strains	L	D	L	D	L	D
S. aureus	>25	>25	6.25	25	6.25	12.5
S. epidermidis	>25	>25	3.13	12.5	3.13	12.5
E. coli	>25	>25	6.25	25	3.13	≥25

[a]Labels D and L stand for dark and light, respectively. [b]Values as high as 2 mM have been reported under similar conditions.[18]

added. This strategy will allow for synergistic inhibitory properties.

Although experiments above attest the microbial inhibition via AuNP@Ag@Asm, a kinetic study of antibacterial activity was also performed for the three strains during a period of 18 h at MIC concentrations. Bactericidal activity denotes 99.9% killing of inoculum with a particular antimicrobial agent. Time−kill curves were constructed by plating bacterial cultures containing the antimicrobial agent at specific time intervals (0−18 h). Four different conditions were considered: (1) AuNP@Ag@Asm at MIC concentration under 530 nm irradiation; (2) AuNP@Ag@Asm at MIC concentration in the dark; (3) no AuNP@Ag@Asm and 530 nm irradiation; (4) no AuNP@Ag@Asm in the dark.

Irradiated and nonirradiated experiments were conducted to measure bactericidal capabilities for AuNP@Ag@Asm and the photothermal activity of gold. The results obtained are shown in Figure 5. They reveal that in the dark cell killing is incomplete (even when below the detection limit), as cells eventually recover. In contrast, illumination causes complete cell death, with no hint of recovery.

As previously mentioned, for each bacteria strain, two control experiments were performed, both in the absence of AuNP@Ag@Asm, under 530 nm irradiation, and in the dark. In all cases, there are no significant differences between the amounts of survivors. In fact, for the last 6−18 h both controls from the nonirradiated and irradiated experiments, in the absence of AuNP@Ag@Asm, held constant values for the log of CFU/mL (∼5). This further corroborates what was seen in the controls for the MIC experiments: when bacterial cultures are irradiated in the absence of nanoparticles, there is no negative impact on their growth or survival. In other words, there is no direct effect of the light on the microbial growth.

When using AuNP@Ag@Asm, in the absence of light a particular trend was observed. For *E. coli*, a decrease of the bacteria growth was recorded until $t = 6$ h; however, at $t = 9$ h, 12 h, and 18 h, dramatic growth was observed. For *S. aureus* and *S. epidermidis* no survival colonies were apparent at $t = 6$ h; however, a significant amount (difference of >3 $\log_{10}$-fold) of bacterial colonies was seen for $t = 18$ h. Thus, almost complete bactericidal activity was seen at $t = 6$ h for nonirradiated experiments, but a significant amount of colonies were seen at $t = 18$ h suggesting loss of bactericidal activity. This may be explained considering that as much as 0.01% of the inoculum could remain after 6 h and grow for the remaining time. The mere presence of AuNP@Ag@Asm is not sufficient for a complete kill of the bacteria. In contrast, irradiated experiments in the presence of AuNP@Ag@Asm (Figure 5, blue bars) show efficient bactericidal activity. At $t = 6$ h, no survival colonies were counted as well as a difference of 3 $\log_{10}$-fold was recorded. This trend was maintained also after $t = 18$ h. Therefore, the antimicrobial contribution of silver is supplemented by irradiation of AuNP@Ag@Asm leading to lasting antimicrobial efficiency. Therefore, it is the combination of the silver antibacterial properties with the gold photothermal effect that makes AuNP@Ag@Asm a remarkably efficient material.

Cell viability information was obtained employing a colorimetric assay (MTS assay) for aspartame, AuNP@Ag@Asm, AgNP@citrate, and AuNP (see SI). No significative effect on the proliferation of primary dermal human skin fibroblasts at different concentrations of AuNP@Ag@Asm was observed. However, a slightly lower proliferation of cells treated with AgNP (although within the experimental error) was obtained, probably due to the release of Ag^{1+} ions.[19]

dx.doi.org/10.1021/ja510435u | J. Am. Chem. Soc. 2014, 136, 17394−17397

Moreover, TEM images (Figure 6) showed a marked difference in the behavior of *S. aureus* and *E. coli*. After 1 h of incubation, AuNP@Ag@Asm are located around the *S. aureus* membrane, possibly due to an electrostatic interaction with the peptidoglican of this Gram positive strain. However, after the same time of interaction, the AuNP@Ag@Asm form small aggregates inside the *E. coli* bacillus, indicating that possible uptake mechanisms may take place in this case, as it does for AgNP.[9] However, both strains present symptoms of membrane structural damage, which is likely attributed to the antibacterial properties of silver.

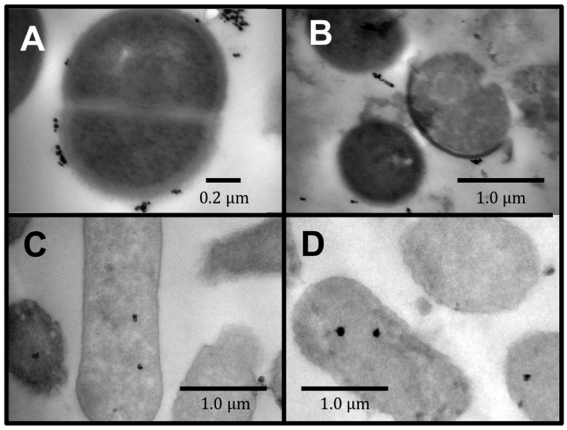

Figure 6. TEM images of *Staphylococcus aureus* ATTC 25923 (A and B) and *Escherichia coli* CF073 (C and D) show the interaction between AuNP@Ag@Asm and the bacterial wall after 1 h of incubation at 37°C.

In conclusion, bimetallic core−shell nanoparticles allow for the exploitation of properties characteristic for monometallic (Au and Ag) nanoparticles. Under irradiation, AuNP@Ag@Asm presented effective inhibitory microbial properties. Further, irradiating the nanoparticles to exploit the photothermal properties of gold was shown to increase inhibitory properties when compared to unirradiated AuNP and AgNP. This finding suggests a synergistic effect between the silver antimicrobial properties and the photothermal effects due to the gold core. The combined effect of silver and gold allowed for complete bactericidal activity whereas noncombinatorial conditions (or nonirradiated experiments) did not. We suggest that thanks to the core−shell nanoparticles synergistic properties, the material proposed represents an attractive antibacterial agent since the photothermal properties of gold can compensate if the silver antimicrobial properties do not suffice for complete bactericidal activity. Aspartame stabilization provides a good shelf life for particles with a material that is nontoxic, inexpensive, and water-soluble.

■ ASSOCIATED CONTENT

Supporting Information

Experimental design for well plate experiments, illumination conditions, EDS data, fibroblasts biocompatibility experiments, and TEM sample preparation details. This material is available free of charge via the Internet at http://pubs.acs.org.

■ AUTHOR INFORMATION

Corresponding Author

scaiano@photo.chem.uottawa.ca

Notes

The authors declare no competing financial interest.

■ ACKNOWLEDGMENTS

C.F. gratefully acknowledges support from NSERC and the Vanier CGS program. We acknowledge the Natural Sciences and Engineering Research Council of Canada, the Canada Research Chairs Program and the Canadian Foundation for Innovation for generous support of this research. Support from the Secretaría de Ciencia y Tecnología de la Universidad Nacional de Córdoba (SeCyT-UNC) and Ministerio de Ciencia y Tecnología (MINCyT, Argentina) is gratefully acknowledged. We acknowledge Dr. Cristina Maldonado for assistance with TEM assays.

■ REFERENCES

(1) Mie, G. *Ann. Physik* **1908**, *330*, 377−445. Burda, C.; Chen, X.; Narayanan, R.; El-Sayed, M. A. *Chem. Rev.* **2005**, *105*, 1025−1102.
(2) Eustis, S.; El-Sayed, M. A. *Chem. Soc. Rev.* **2006**, *35*, 209−217.
(3) Corma, A.; Garcia, H. *Chem. Soc. Rev.* **2008**, *37*, 2096−2126.
(4) Huang, X. H.; Jain, P. K.; El-Sayed, I. H.; El-Sayed, M. A. *Photochem. Photobiol.* **2006**, *82*, 412−417.
(5) Chatterjee, D. K.; Fong, L. S.; Zhang, Y. *Adv. Drug Delivery Rev.* **2008**, *60*, 1627−1637.
(6) Fasciani, C.; Bueno Alejo, C. J.; Grenier, M.; Netto-Ferreira, J. C.; Scaiano, J. C. *Org. Lett.* **2011**, *13*, 204−207.
(7) Agostinis, P.; Berg, K.; Cengel, K. A.; Foster, T. H.; Girotti, A. W.; Gollnick, S. O.; Hahn, S. M.; Hamblin, M. R.; Juzeniene, A.; Kessel, D.; Korbelik, M.; Moan, J.; Mroz, P.; Nowis, D.; Piette, J.; Wilson, B. C.; Golab, J. *CA: Cancer J. Clin.* **2011**, *61*, 250−281. Sperandio, F.; Huang, Y.; Hamblin, M. *Antiinfect. Drug Discov.* **2013**, *8*, 108−120.
(8) Alarcon, E.; Bueno-Alejo, C.; Noel, C.; Stamplecoskie, K.; Pacioni, N.; Poblete, H.; Scaiano, J. C. *J. Nanopart. Res.* **2013**, *15*, 1−14. Kalishwaralal, K.; BarathManiKanth, S.; Pandian, S. R. K.; Deepak, V.; Gurunathan, S. *Colloids Surf. B: Biointerfaces* **2010**, *79*, 340−344.
(9) Mukherjee, S.; Chowdhury, D.; Kotcherlakota, R.; Patra, S.; Vinothkumar, B.; Bhadra, M. P.; Sreedhar, B.; Patra, C. R. *Theranostics* **2014**, *4*, 316−335.
(10) Vignoni, M.; de Alwis Weerasekera, H.; Simpson, M. J.; Phopase, J.; Mah, T.-F.; Griffith, M.; Alarcon, E. I.; Scaiano, J. C. *Nanoscale* **2014**, *6*, 5725−5728.
(11) McGilvray, K. L.; Fasciani, C.; Bueno-Alejo, C. J.; Schwartz-Narbonne, R.; Scaiano, J. C. *Langmuir* **2012**, *28*, 16148−16155.
(12) Gonzalez, C. M.; Liu, Y.; Scaiano, J. C. *J. Phys. Chem. C* **2009**, *113*, 11861−11867.
(13) Baffou, G.; Quidant, R. *Laser Phot. Rev.* **2013**, *7*, 171−187. Khaing Oo, M. K.; Yang, Y.; Hu, Y.; Gomez, M.; Du, H.; Wang, H. *ACS Nano* **2012**, *6*, 1939−1947.
(14) Magnuson, B. A.; Burdock, G. A.; Doull, J.; Kroes, R. M.; Marsh, G. M.; Pariza, M. W.; Spencer, P. S.; Waddell, W. J.; Walker, R.; Williams, G. M. *Crit. Rev. Toxicol.* **2007**, *37*, 629−727. Butchko, H. H.; Stargel, W. W.; Comer, C. P.; Mayhew, D. A.; Benninger, C.; Blackburn, G. L.; de Sonneville, L. M. J.; Geha, R. S.; Hertelendy, Z.; Koestner, A.; Leon, A. S.; Liepa, G. U.; McMartin, K. E.; Mendenhall, C. L.; Munro, I. C.; Novotny, E. J.; Renwick, A. G.; Schiffman, S. S.; Schomer, D. L.; Shaywitz, B. A.; Spiers, P. A.; Tephly, T. R.; Thomas, J. A.; Trefz, F. K. *Regul. Toxicol. Pharmacol.* **2002**, *35*, S1−S93.
(15) McGilvray, K. L.; Decan, M. R.; Wang, D.; Scaiano, J. C. *J. Am. Chem. Soc.* **2006**, *128*, 15980−15981.
(16) Scaiano, J. C.; Billone, P.; Gonzalez, C. M.; Maretti, L.; Marin, M. L.; McGilvray, K. L.; Yuan, N. *Pure Appl. Chem.* **2009**, *81*, 635−647.
(17) Scaiano, J. C.; Stamplecoskie, K. G.; Hallett-Tapley, G. L. *Chem. Commun.* **2012**, *48*, 4798−4808.
(18) Silvero, M. J.; Argüello, G. A.; Becerra, M. C. *J. Nanopharm. Drug Delivery* **2014**, *2*, 1−5.
(19) Bartlomiejczyk, T.; Lankoff, A.; Kruszewski, M.; Szumiel, I. *Ann. Agr. Env. Med.* **2013**, *20*, 48−54.